An Effective Pathway to Design and Synthesize UV Birefringent Crystals via Rational Assemble of π-Conjugated [CO3]2− and [NO3]− Triangles

Journal:	*Journal of Materials Chemistry C*
Manuscript ID	TC-ART-12-2022-005374.R1
Article Type:	Paper
Date Submitted by the Author:	28-Jan-2023
Complete List of Authors:	Hu, Zhaowei; Shanghai Institute of Technology, School of Materials science and Engineering Liu, Lili; Shanghai Institute of Technology, School of Materials science and Engineering Zhang, Ruixin; Xinjiang University Jing, Qun; Xinjiang University, School of Physical Science and Technology Wang, Huan; Shanghai Institute of Technology, School of Materials science and Engineering tian, jindan; Shanghai Institute of Technology, School of Materials Science and Engineering Xu, Jiayue; Shanghai Institute of Technology, Halasyamani, P.; University of Houston, Chemistry

SCHOLARONE™
Manuscripts

ARTICLE

An Effective Pathway to Design and Synthesize UV Birefringent Crystals via Rational Assemble of π-Conjugated $[CO_3]^{2-}$ and $[NO_3]^-$ Triangles

Zhaowei Hu,[a] Lili Liu,*[a] Ruixin Zhang,[b] Qun Jing,[b] Huan Wang,[a] Jindan Tian,[a] Jiayue Xu,*[a] and P. Shiv Halasyamani*[c]

Planar MO_3 (M=B, C, N) units have frequently been considered as the important structural components of novel birefringent crystal materials. An efficient approach for creating new functional crystals is to simultaneously assemble multiple structural motifs together. Two compounds, $Na_3Rb_6(CO_3)_3(NO_3)_2X\cdot6H_2O$ (X = Br and Cl), were synthesized by the integration of three kinds of anionic groups. More interestingly, $[CO_3]^{2-}$ and $[NO_3]^-$ groups in $Na_3Rb_6(CO_3)_3(NO_3)_2X\cdot6H_2O$ are all coplanar under the guidance of $[NaO_7]^{13-}$ polyhedra, which can enhance the anisotropic polarizability. $Na_3Rb_6(CO_3)_3(NO_3)_2X\cdot6H_2O$ have large theoretical birefringence of ~0.165 at 1064 nm and possess short UV cut-off edge of ~230 nm. Additionally, the two compounds exhibit good crystal growth habits. These properties illustrate that $Na_3Rb_6(CO_3)_3(NO_3)_2X\cdot6H_2O$ are promising UV birefringent crystals.

Introduction

UV birefringent crystals, as a type of important functional material for optoelectronics, have important applications in optical deflection, optical modulation, and nonlinear optics.[1-5] At present, commercial UV birefringent crystals, such as $CaCO_3$,[6] α-BaB_2O_4 (α-BBO)[7] and MgF_2,[8] have been facing kinds of problems, like difficulty in crystal growth, small birefringence, insufficient band gap, which seriously limit their practical applications. Therefore, new high-performance UV birefringent crystals are still needed.

Previous studies mainly focused on borate UV birefringent crystals,[9-12] such as $SrAlB_3O_6F_2$ (0.078 at 1064 nm, 7.65 eV),[13] $Li_3La_2(BO_3)_3$ (0.078 at 1064 nm, 5.22 eV),[14] $Ca(BO_2)_2$ (0.247 at 193 nm, 7.34 eV),[15] $Ba_2Zn_2B_6O_{13}$ (0.085 at 532 nm, 6.12 eV),[16] $NaMgBe_2(BO_3)_2F$ (0.078 at 589 nm, 4.19 eV),[17] which is mainly attributed to the excellent properties of the planar triangle $[BO_3]^{3-}$ group, including relatively strong anisotropic polarizability and high UV transmittance.[18-21] It is well known that $[CO_3]^{2-}$ and $[NO_3]^-$ groups possess the similar π-conjugated electronic configuration and planar triangle structure as $[BO_3]^{3-}$ group.[22,23] In terms of the anisotropic polarizability of anionic groups, it generally follows the trend of $[NO_3]^- > [CO_3]^{2-} > [BO_3]^{3-}$.[24] Therefore, $[CO_3]^{2-}$ and $[NO_3]^-$ groups are also ideal fundamental building blocks (FBBs) for designing birefringent materials, and they have advantages over $[BO_3]^{3-}$ group when building birefringent materials.[25]

After reviewing the inorganic crystal structure database (ICSD with the version of 4.9.0. the last release of ICSD-2022.2), we find that there have been relatively more borate carbonates reported, but fewer nitrate borates and nitrate carbonates. Through extensive literature research, it is noticed that the pH value for synthesizing nitrate is often different from that for borate/carbonate when using solution methods. Many of the reported nitrates are synthesized under acidic conditions, for example, $La(OH)_2NO_3$ (pH 4-6),[26] $[Pb_4(OH)_4](NO_3)_4$ (pH 4-5),[27] $BiGeO_2(OH)_2NO_3$ (pH ≈ 0.2),[28] etc. In contrast, hexagonal H_3BO_3 crystals will deposit from borate system and $[CO_3]^{2-}$ will be decomposed into CO_2 molecule from carbonate system under acidic environment. Therefore, the coexistence of these three groups is difficult to reconcile. In recent years, there are several compounds recorded in BO_3-CO_3 and BO_3-NO_3 systems, such as $Pb_7O(OH)_3(CO_3)_3(BO_3)$,[29] $Rb_9[B_4O_5(OH)_4]_3(CO_3)Br\cdot7H_2O$,[30] $Ba_3(BO_3)(CO_3)F$,[31] $K_3(B_6O_{10})(NO_3)$,[32] $Pb_6O_4(BO_3)(NO_3)$[33] and $Pb_2(BO_3)(NO_3)$,[34] while carbonate nitrates are rarely reported. In the ICSD, there are only ten compounds containing both $[CO_3]^{2-}$ and $[NO_3]^-$ groups been reported before 2022, and their physical and chemical properties are less studied (shown in Table 1). In particular, their optical properties (like birefringence, SHG effect) have not been systematically studied.

Metal-centered polyhedra also have impacts on the structure and optical properties of crystals. Like stereochemically active lone pair (SCALP) cations or d^0 metal cations, they can positively affect the

[a.] Institute of Crystal Growth, School of Materials Science and Engineering, Shanghai Institute of Technology, Shanghai 201418, China.
E-mail: liulili@sit.edu.cn; xujiayue@sit.edu.

[b.] School of Physical Science and Technology, Xinjiang University, Urumqi 830046, China.

[c.] Department of Chemistry, University of Houston, 112 Fleming Building, Houston, Texas 77204, USA.
Email: psh@uh.edu

ARTICLE

Table 1 Compounds in CO_3-NO_3 system before 2022.

Compounds	Space group	Year
$[Co(NH_3)_4(CO_3)(NO_3)]_2 \cdot H_2O$[35]	$P2_1/n$	1990
$[Pt(NH_3)_2]_4(CO_3)_2(NO_3)_4 \cdot 3H_2O$[36]	$P\overline{1}$	1993
$(Tl_{0.85}Cr_{0.15})Sr_4Cu_2(CO_3)_{0.5}(NO_3)_{0.5}O_7$[37]	$P4/mmm$	1997
$(NH_3)_3Co(OH)_2(CO_3)Co(NH_3)_3(NO_3)_2 \cdot H_2O$[38]	$P\overline{1}$	1999
$Co(NH_3)_5(CO_3)NO_3 \cdot H_2O$[39]	$P2_1$	1999
$(Pb_6O_4)(OH)(NO_3)(CO_3)$[40]	$Pnma$	2000
$PbTiO_2(CO_3)_{0.3}(NO_3)_{0.35}(OH)$[41]	$P\overline{3}1m$	2001
$Ca_5(UO_2(CO_3)_3)_2(NO_3)_2 \cdot 10H_2O$[42]	$P2_1/n$	2002
$Co(CO_3)(NH_3)_4NO_3$[43]	$P2_1/c$	2013
$(NH_3)_6Rh_2(CO_3)(OH)_2(NO_3)_2 \cdot H_2O$[44]	$P\overline{1}$	2016

birefringence,[45,46] such as SCALP Sn^{2+} atom in Sn_2PO_4I (0.664 at 532nm),[47] $[WO_5F]^{5-}$ octahedron in KWO_3F (0.088 at 1064nm),[48] etc. However, these metal cations play a negative role in the transmission of UV light.[49] During the design and syntheses of UV birefringent crystals, alkali or alkaline earth metals are the preferred elements owing to the absence of electron transition of *d-d* and *f-f* orbitals, which can effectively extend the band gap.[50,51] Furthermore, compared with O^{2-} ion, halogen anions (F^-, Cl^-, Br^-) possess distinctive electronegativity, coordination ability and polarizability. So halogenated oxypolyhedra (like $[BO_3F]^{4-}$, $[TiO_5F]^{7-}$, $[WO_5F]^{5-}$ groups) always exhibit larger polarizability than oxypolyhedra (like $[BO_4]^{5-}$, $[TiO_6]^{8-}$, $[WO_6]^{6-}$ groups). Additionally, the addition of halogen anions usually can make the UV cutoff edge blue-shift.[52]

Guided by above ideas, we successfully synthesized two mixed-alkali metal carbonate nitrate halides, $Na_3Rb_6(CO_3)_3(NO_3)_2X \cdot 6H_2O$ (X = Br and Cl), through hydrothermal method. We noticed during our manuscript preperation that, quite recently, the $Na_3Rb_6(CO_3)_3(NO_3)_2Cl \cdot 6H_2O$ was synthesized via evaperation method by Pan's group.[53] Therefore, in this work, we will mainly focus on the synthesis and properties of $Na_3Rb_6(CO_3)_3(NO_3)_2Br \cdot 6H_2O$, but $Na_3Rb_6(CO_3)_3(NO_3)_2Cl \cdot 6H_2O$ is also briefly described and characterized for comparison. And $Na_3Rb_6(CO_3)_3(NO_3)_2Br \cdot 6H_2O$ is the first crabonate nitrate bromide. $Na_3Rb_6(CO_3)_3(NO_3)_2X \cdot 6H_2O$ contains four different functional primitives, which includes alkali metals (Na^+ and Rb^+), $[CO_3]^{2-}$, $[NO_3]^-$ and halogen anions. Their synergistic effect gives $Na_3Rb_6(CO_3)_3(NO_3)_2X \cdot 6H_2O$ excellent linear optical properties: large birefringences and wide UV optical band gaps. Besides, they have no layered growth habit and it is feasible to obtain millimeter sized crystals, ensuring the availability of large-scale single crystals. Therefore, they have the potential to serve as excellent UV birefringent crystals.

Experimental

Reagents. $Ce(NO_3)_3 \cdot 6H_2O(99\%)$, $Rb_2CO_3(99\%)$, $NaOH(99\%)$, $NaBr(99\%)$, $NaCl(99\%)$ were purchased from Taitan and used as received.

Synthesis. Considering that the $[CO_3]^{2-}$ group is not stable in acidic solutions, we will try to combine $[CO_3]^{2-}$ and $[NO_3]^-$ groups under neutral or alkaline conditions. Although nitrates tend to form under acidic conditions, there are still examples synthesized under alkaline conditions, such as $Pb_2O(OH)NO_3$ (pH = 7~8) and $Pb_3O_2(OH)NO_3$ (pH = 11).[27] After constant adjustment of raw materials and ratios, $Na_3Rb_6(CO_3)_3(NO_3)_2X \cdot 6H_2O$ was finally synthesized using hydrothermal method. In the synthesis of $Na_3Rb_6(CO_3)_3(NO_3)_2Br \cdot 6H_2O$, the reaction mixture of $Ce(NO_3)_3 \cdot 6H_2O$ (1.520 g, 3.5 mmol), Rb_2CO_3 (3.002 g, 13 mmol), NaOH (0.500 g, 12.5 mmol), NaBr(1.029 g, 10 mmol) and 5 mL deionized water were sealed in an autoclave with a 23 mL Teflon linear. After heating at 220 °C for 2 days, the reactant was cooled to room temperature at a rate of 3 °C/h. Similarly, single crystals of $Na_3Rb_6(CO_3)_3(NO_3)_2Cl \cdot 6H_2O$ were synthesized with a reaction mixture of $Ce(NO_3)_3 \cdot 6H_2O$ (1.086 g, 2.5 mmol), Rb_2CO_3 (3.464 g, 15 mmol), NaOH (0.800 g, 20 mmol), NaCl (0.584 g, 10 mmol) and 5 ml deionized water. Colorless and block crystals (Figure S1) were obtained after washing by deionized water or ethanol. The polycrystalline powder samples of $Na_3Rb_6(CO_3)_3(NO_3)_2Br \cdot 6H_2O$ and $Na_3Rb_6(CO_3)_3(NO_3)_2Cl \cdot 6H_2O$ were obtained directly from grinding the as-grown crystals, and their purity was checked by powder X-ray diffraction patterns (see Figure S2).

Single crystal X-ray diffraction. Single crystal X-ray diffraction data of $Na_3Rb_6(CO_3)_3(NO_3)_2Br \cdot 6H_2O$ and $Na_3Rb_6(CO_3)_3(NO_3)_2Cl \cdot 6H_2O$ were collected at room temperature by single-crystal XRD on an APEX II CCD diffractometer using monochromatic Mo-Kα radiation (λ=0.71073 Å). A transparent block of crystal was mounted on a glass fiber with epoxy for structure determination. Moreover, absorption corrections were carried out using the SCALE program for area detector and integrated with the SAINT program.[54] Absorption corrections based on the multi-scan technique were also applied. The structure was solved by the direct method and refined by full-matrix least-squares fitting on F^2 by SHELX-97.[55] All H atoms are located at geometrically calculated positions and refined with isotropic thermal parameters. All the other atoms were refined anisotropically. All the structural data were also checked for possible missing symmetry with the program PLATON,[56] and no higher symmetries were found. Relevant crystallographic data and details of the experimental conditions for $Na_3Rb_6(CO_3)_3(NO_3)_2Br \cdot 6H_2O$ and $Na_3Rb_6(CO_3)_3(NO_3)_2Cl \cdot 6H_2O$ are summarized in Table S1. Further details about atomic coordinates and isotropic displacement coefficients are supplied in Tables S2 - S3. Selected bond lengths are listed in Tables S4 - S5. Hydrogen coordinates and isotropic displacement parameters are listed in Tables S6 - S7.

Powder X-ray diffraction (PXRD). PXRD patterns of polycrystalline materials were obtained on a TD-3500 X-ray diffractometer by using Cu Kα radiation (λ=1.540598 Å) at room temperature in the angular range of 2θ = 10 - 70° with a scan step width of 0.05° and a fixed time

of 0.2 s. The PXRD patterns for the pure samples of $Na_3Rb_6(CO_3)_3(NO_3)_2Br\cdot6H_2O$ and $Na_3Rb_6(CO_3)_3(NO_3)_2Cl\cdot6H_2O$ show good agreement with the calculated PXRD patterns from the single-crystal models (see Figure S2).

Thermal analysis. Thermogravimetric analysis (TG) and differential scanning calorimetry (DSC) were conducted on Mettler Toledo unit. The crystal samples (5-12 mg) were enclosed in Al_2O_3 crucibles and heated from room temperature to 800 °C at a rate of 10 °C/min under a constant flow of nitrogen gas.

Infrared spectroscopy. IR spectra were recorded on a Thermo Fisher Scientific Fourier transform infrared (FT-IR) spectrometer as KBr pellets in the range of 4000-400 cm^{-1}.

UV-vis diffuse reflectance spectroscopy. The UV-vis diffuse reflection data were recorded at room temperature using powder samples on a Varian Cary 5000 UV/vis/NIR spectrophotometer and scanned at 200-800 nm. $BaSO_4$ acts as the standard.

Birefringence. The birefringence (Δn) of $Na_3Rb_6(CO_3)_3(NO_3)_2Br\cdot6H_2O$ was characterized by using a polarization microscope equipped (ZEISS Axio Scope. 5 pol) with a Berek compensator. The average wavelength of the light source was 546 nm. The equation for calculating the birefringence is listed below,

$$R = |N_g - N_p| \times d = \Delta n \times d$$

Here, R represents the optical path difference; N_g, N_p and Δn mean the refractive index of fast light, slow light, and the difference value of the refractive index, respectively; d denotes the thickness of the crystal.

Computational descriptions. The first-principles calculations for $Na_3Rb_6(CO_3)_3(NO_3)_2X\cdot6H_2O$ (X = Br and Cl) crystal were performed by the plane-wave pseudopotential method implemented in CASTEP[57] program based on density functional theory (DFT)[58] with the norm-conserving pseudopotentials (NCP).[59] The exchange-correlation (XC) functional were described by the Perdew-Burke-Ernzerhof(PBE) functional within the generalized gradient approximation (GGA).[60] The crystal structure of $Na_3Rb_6(CO_3)_3(NO_3)_2X\cdot6H_2O$ was optimized until the total energy, the maximum stress, the maximum atomic displacements and the maximum force were smaller than 5×10^{-6} eV/atom, 2×10^{-2} GPa, 5×10^{-4} Å, less than 1×10^{-2} eV/Å, respectively. The following valence electron configurations were used: $H(1s^1)$, $C(2s^22p^2)$, $N(2s^22p^3)$, $O(2s^22p^4)$, $Na(2s^22p^63s^1)$, $Cl(3s^23p^5)$, $Rb(4s^24p^65s^1)$ for $Na_3Rb_6(CO_3)_3(NO_3)_2Cl\cdot6H_2O$ and $H(1s^1)$, $C(2s^22p^2)$, $N(2s^22p^3)$, $O(2s^22p^4)$, $Na(2s^22p^63s^1)$, $Br(4s^24p^5)$, $Rb(4s^24p^65s^1)$ for $Na_3Rb_6(CO_3)_3(NO_3)_2Br\cdot6H_2O$. And the plane-wave energy cut-off was both set at 830.0 eV. The k-point of Monkhorst-Pack grid in the Brillouin zone for $Na_3Rb_6(CO_3)_3(NO_3)_2X\cdot6H_2O$ were set as 3×3×2 and the span of the Brillouin zone were selected as 0.04 $Å^{-1}$ which ensure the sufficient accuracy of the calculated results. It is well-known that GGA method always underestimates the bandgap owing to the discontinuity of exchange-correlation energy functional, hence a so-called scissors operator was used to calculate the optical properties.

Results and discussion

Structure description. $Na_3Rb_6(CO_3)_3(NO_3)_2Br\cdot6H_2O$ crystallizes in the centrosymmetric space group $P6_3/mcm$ (No. 194, Table S1). In its asymmetric unit, there is one Na atom, one Rb atom, one N atom, two C atoms, four O atoms, one Br atom and one H atom (Figures S3 and S4). $Na_3Rb_6(CO_3)_3(NO_3)_2Br\cdot6H_2O$ exhibits a three-dimensional (3D) crystal structure consisting of $[NaO_7]^{13-}$, $[BrRb_6]^{5+}$, $[CO_3]^{2-}$, $[NO_3]^-$ and H_2O units (Figure 1a). Each Na atom is coordinated to seven O atoms as $[NaO_7]^{13-}$ pentagon double cone, five of which are equatorial O atoms and the rest two are apical O atoms (Figure S5). In $[NaO_7]^{13-}$, the five equatorial O atoms are connected to two edge-shared $[NO_3]^-$ and one corner-shared $[C(1)O_3]^{2-}$, and the two apical O atoms are linked to H atoms to form two H_2O groups. And then the $[Na(CO_3)(NO_3)_2\cdot2H_2O]^{4-}$ polyhedron are formed, which extends infinitely in ab plane to create the 2D $[Na_3(CO_3)(NO_3)_2\cdot2H_2O]- \infty$ layer (Figure 1b). The distance between adjacent $[Na_3(CO_3)(NO_3)_2\cdot2H_2O]- \infty$ layers (d_{Br}) is 7.93 Å. Each Br atom is surrounded by six Rb atoms to form $[BrRb_6]^{5+}$ cationic octahedron (Figure S6). $[BrRb_6]^{5+}$ octahedra and $[C(2)O_3]^{2-}$ units are further connected with each other to compose the $[(Rb_6Br)(CO_3)_2]+ \infty$ layers via Rb-O bonds (Figure 1c). Moreover, $[C(2)O_3]^{2-}$ groups are also parallel to the ab plane under the guidance of $[BrRb_6]^{5+}$. Eventually, $[Na_3(CO_3)(NO_3)_2\cdot2H_2O]- \infty$ layers and $[(Rb_6Br)(CO_3)_2]+ \infty$ layers are stacked alternately along the c-axis to construct the whole structure of $Na_3Rb_6(CO_3)_3(NO_3)_2Br\cdot6H_2O$. In connectivity terms, the material may be described as $3[Na(CO_3)_{1/3}2(NO_3)_{1/3}\cdot2H_2O]^{1/3-}$ anion, with charge balance maintained by $[(Rb_6Br)6(CO_3)_{1/3}]^+$ cation. Compared with $Na_3Rb_6(CO_3)_3(NO_3)_2Br\cdot6H_2O$, the layer spacing of isostructural $Na_3Rb_6(CO_3)_3(NO_3)_2Cl\cdot6H_2O$ (d_{Cl}, Figure 1d) decreases from 7.93 Å to 7.91 Å due to the replacement of the Br^- ion by smaller Cl^- ion.

In $Na_3Rb_6(CO_3)_3(NO_3)_2Br\cdot6H_2O$, Na-O distances are in the range of 2.303(4) - 2.683(5) Å. The C-O bond distances range from 1.281(2) to 1.285(4) Å. The N-O bond distance is 1.254(4) Å. The Rb^+ cation is surrounded by eight O atoms and one Br atom, with Rb-O distances of 3.012(2) - 3.413(3) Å and Rb-Br distance of 3.344(1) Å. All bond lengths are within reasonable limits. The bond valence of the crystalline elements is determined by the following equation,

$$V_i = \sum_j s_{ij} = \sum_j exp\{(r_0 - r_{ij})/B\}$$

where S_{ij} is an empirical determined parameter related to the bond lengths r_0, r_{ij} and B (usually 0.37).[61,62] Bond valence sums (BVSs) calculations indicate that BVSs for Na, Rb, C(1) - C(2), N, O(1) - O(4) and Br are +1.178, +1.130, +3.992 - +4.282, +4.817, −0.463 - −2.105, −1.307, respectively (Table S2). Wherein, O(1) has smaller BVS value (−0.463), so it is determined to be connected with H atoms to form H_2O molecule. The elemental bond valence of $Na_3Rb_6(CO_3)_3(NO_3)_2Cl\cdot6H_2O$ is listed in Table S3.

Structure-property relationship. π-conjugated groups, MO_3 (M=B, N and C), are ideal functional motifs for birefringent materials because of their large anisotropic polarizability. The appropriate arrangement of MO_3 groups has a strong influence on the macroscopic optical properties of crystals. For example, compounds $NaZnCO_3F$ and $Na_4Zn(CO_3)_3$, reported by Ye's group, have the same functional unit of π-conjugated $[CO_3]^{2-}$ group. In terms of their crystal structures, the

$[CO_3]^{2-}$ in $NaZnCO_3F$ are arranged in coplanar manner, but $[CO_3]^{2-}$ groups in $Na_4Zn(CO_3)_3$ point in different directions.[63] The different arrangements of $[CO_3]^{2-}$ groups make $NaZnCO_3F$ have a larger birefringence of 0.171 at 1064 nm, and $Na_4Zn(CO_3)_3$ have a relatively smaller birefringence of 0.138 at 1064 nm. Therefore, coplanar arrangement is the optimum choice, which can promote effective superposition of microcosmic anisotropic polarizability.

Then, how to achieve the coplanar arrangement of MO_3 group? From the well-known $ABCO_3F$ system, it can be realized that the equatorial O atoms can efficiently direct MO_3 for coplanar arrangement. Moreover, we found that the oxypolyhedra formed by divalent metal cations can provide equatorial O atoms, such as Sr^{2+} in $RbSrCO_3F^{64}$ (Figure 2a) and $Sr_2(OH)_3NO_3$ (Figure 2b),[65] Mg^{2+} in $RbMgCO_3F$ (Figure 2c),[66] Cd^{2+} in and $KCdCO_3F$ (Figure 2d),[67] Pb^{2+} in $CsPbCO_3F$ (Figure 2e).[68] But it is rarely reported that alkali metal-centered oxypolyhedra offer equatorial O atoms. Interestingly, $[NaO_7]^{13-}$ polyhedron in $Na_3Rb_6(CO_3)_3(NO_3)_2Br\cdot6H_2O$ (this work) has five equatorial O atoms, and same situation happened in $Na_3Rb_6(CO_3)_3(NO_3)_2Cl\cdot6H_2O$, which prompts us to study related systems (Figure 1a). We investigated two systems including mixed-alkali metal carbonates and mixed-alkali metal nitrates to study the phenomenon of alkali metal cations supplying equatorial O atoms. There are eleven compounds in the two systems according to ICSD database (listed in Table 2), and only five of them possess equatorial O atoms: $NaRb_2(NO_3)_3$,[69] $NaA_2(HCO_3)(CO_3)\cdot2H_2O$ (A = K and Rb)[70] and $Na_3Rb_6(CO_3)_3(NO_3)_2Cl\cdot6H_2O$,[53] $Na_3Rb_6(CO_3)_3(NO_3)_2Br\cdot6H_2O$ (this work). In $NaRb_2(NO_3)_3$, Na^+ is connected with eight O atoms, six of which are equatorial O atoms from three bidentate $[NO_3]^-$. While in $NaA_2(HCO_3)(CO_3)\cdot2H_2O$, Na^+ is bonded to six O atoms, and only four of them are equatorial O atoms linking with two bidentate $[CO_3]^{2-}$. However, Na^+ in $Na_3Rb_6(CO_3)_3(NO_3)_2X\cdot6H_2O$ has five equatorial O

atoms, four of which are from two bidentate $[NO_3]^-$ groups and the rest one is from a monodentate $[CO_3]^{2-}$ group. Through literature research and structural comparison, it was found that Na^+ in $Na_3Rb_6(CO_3)_3(NO_3)_2X\cdot6H_2O$ (this work) is similar to Ca^{2+} in $RbCaCO_3F^{64}$ from $ABCO_3F$ family, and both of them are seven coordinated and have five equatorial O atoms to direct MO_3 groups to be coplanar (Figure 3).

A proper ionic radius has an essential effect on the formation of equatorial O atoms. In Table 2, it is noticed that the cation with too large or small radius does not have equatorial atoms. For example, Li^+ ions in $LiACO_3$ (A=Na, K, Rb, Cs) are four or five-coordinated, and these $[LiO_4]^{7-}$ or $[LiO_5]^{9-}$ groups do not have equatorial atoms, which is probably because Li atom is too small to bond with enough O atoms to form the equatorial plane. If the cation radius is too large, it will impede the formation of equatorial plane, because large cations usually may attract too many O atoms as ligands and make the O atoms deviate from the equatorial plane, like A'' atoms in Table 2. Therefore, the cations with moderate radius can promote the construction of equatorial O plane and then guide the arrangement of planar MO_3 groups. It is found that all the equatorial O atoms appear in the Na-centered polyhedra in Table 2, which demonstrates that Na^+ possesses a suitable ionic radius. Inspired by Zou's work,[64] we speculated that the number of equatorial O atoms is related to the radius ratio of different cations. So, we calculated the cation radius ratio (A''/A' ratio) of the compounds listed in Table 2. It illustrates that when A''/A' ratio is between 1.386 - 1.509, equatorial O atoms will appear, otherwise, they will not exist. In addition, the number of equatorial O decreases with the increase of the A''/A' ratio. Therefore, the choice of cation is crucial in design and synthesis of planar group optical materials, which has a significant effect on the structure and properties of materials.
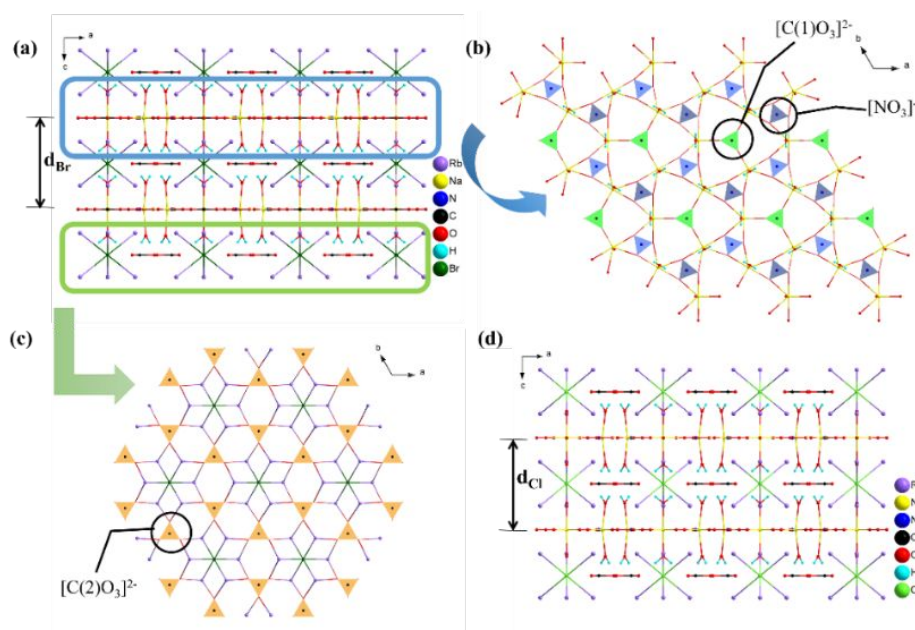
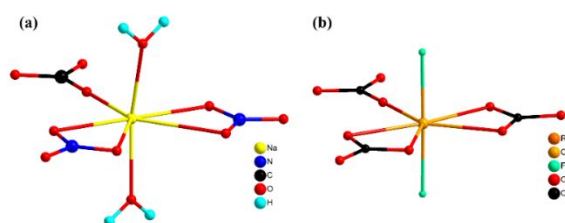**Figure 1** (a) The crystal structure of $Na_3Rb_6(CO_3)_3(NO_3)_2Br\cdot6H_2O$; (b) $[Na_3(CO_3)(NO_3)_2\cdot2H_2O]-\infty$ layer; (c) $[(Rb_6Br)(CO_3)_2]+\infty$ layer; (d) The crystal structure of $Na_3Rb_6(CO_3)_3(NO_3)_2Cl\cdot6H_2O$. (Rb-O bonds are omitted for clarity)
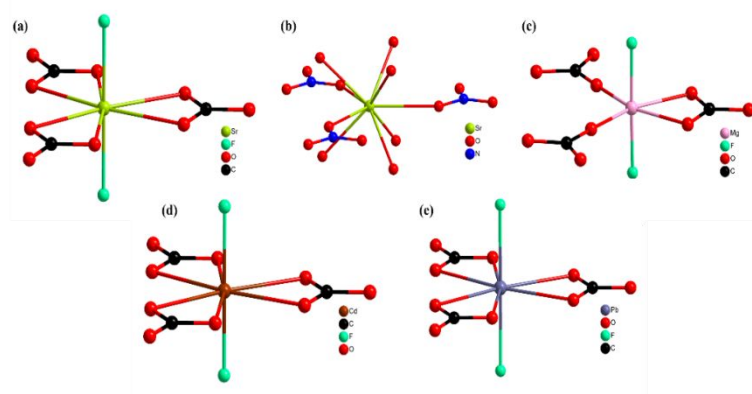
Figure 2 The coordination environments of Sr^{2+} in $RbSrCO_3F$ (a), Sr^{2+} in $Sr_2(OH)_3NO_3$ (b), Mg^{2+} in $RbMgCO_3F$ (c), Cd^{2+} in and $KCdCO_3F$ (d) and Pb^{2+} in $CsPbCO_3F$ (e)

Figure 3 The coordination environments of (a) Na^+ in $Na_3Rb_6(CO_3)_3(NO_3)_2Br·6H_2O$ and (b) Ca^{2+} in $RbCaCO_3F$.

Table 2 Mixed-alkali metal carbonates and mixed-alkali metal nitrates. (A'= alkali metals with smaller atomic numbers; A''= alkali metals with bigger atomic numbers)

Molecular formula	A'	A''	A''/A'	A'O$_n$ unit	A''O$_n$ unit	Equatorial O atoms
KRb_2CO_3F[71]	K	Rb		Disordered structure		
$LiNaCO_3$[72]	Li	Na	1.562			None
$LiKCO_3$[73]	Li	K	2.192			None
$LiRbCO_3$[73]	Li	Rb	2.329			None
$LiCsCO_3$[73]	Li	Cs	2.671			None
$NaKCO_3·6H_2O$[74]	Na	K	1.310			None
$NaK_2(HCO_3)(CO_3)·2H_2O$[70]	Na	K	1.422			Four
$NaRb_2(HCO_3)(CO_3)·2H_2O$[70]	Na	Rb	1.509			Four

Na$_3$Rb$_6$(CO$_3$)$_3$(NO$_3$)$_2$Cl·6H$_2$O[53]	Na	Rb	1.452			Five
Na$_3$Rb$_6$(CO$_3$)$_3$(NO$_3$)$_2$Br·6H$_2$O[a]	Na	Rb	1.452			Five
NaRb$_2$(NO$_3$)$_3$[69]	Na	Rb	1.386			Six

[a] The compound synthesized in this work.

Thermal Behaviours. The TG-DSC curves of Na$_3$Rb$_6$(CO$_3$)$_3$(NO$_3$)$_2$Br·6H$_2$O are shown in Figure S7a. It is stable until ~100 °C, and the significant weight loss is presumably attributed to the absence of crystal water. The graph shows a weight loss ratio of 9.76%, which is basically consistent with the theoretical calculation 10.06%. The decomposition of Na$_3$Rb$_6$(CO$_3$)$_3$(NO$_3$)$_2$Br·6H$_2$O has also occurred at the same time. The remaining chemicals are mainly RbBr, RbNO$_3$ and Na$_2$CO$_3$ (Figure S8a). And the peak around 350 °C represents the melting point. The weightlessness after 600 °C is due to volatilization of residues. Na$_3$Rb$_6$(CO$_3$)$_3$(NO$_3$)$_2$Cl·6H$_2$O exhibits similar trends (Figure S7b).

IR and UV-vis diffuse reflectance spectra. The IR spectrum of Na$_3$Rb$_6$(CO$_3$)$_3$(NO$_3$)$_2$Br·6H$_2$O is shown in Figure S9a. The stretching of O-H leads to large broad bands at 3104 cm^{-1} and around 2423 cm^{-1}. The stretching vibrations of C-O and N-O can be reflected by the peaks around 1400 cm^{-1}. The out-of-plane and bending vibrations of C-O-C can be observed at 864 cm^{-1} and 702 cm^{-1}, and the peaks at 825 cm^{-1} and 794 cm^{-1} reflect the nonplanar bending vibration of [NO$_3$]$^-$ triangular group. Na$_3$Rb$_6$(CO$_3$)$_3$(NO$_3$)$_2$Cl·6H$_2$O also possesses similar peaks (Figure S9b).

The UV-vis diffuse reflectance spectra of Na$_3$Rb$_6$(CO$_3$)$_3$(NO$_3$)$_2$X·6H$_2$O were measured by using the powder samples. As shown in Figure 4, the reflectance for Na$_3$Rb$_6$(CO$_3$)$_3$(NO$_3$)$_2$Br·6H$_2$O at 230 nm is about 13%, and the value for Na$_3$Rb$_6$(CO$_3$)$_3$(NO$_3$)$_2$Cl·6H$_2$O at 228 nm is about 5%, which illustrates that the UV cut-off edges of Na$_3$Rb$_6$(CO$_3$)$_3$(NO$_3$)$_2$Br·6H$_2$O and Na$_3$Rb$_6$(CO$_3$)$_3$(NO$_3$)$_2$Cl·6H$_2$O are shorter than 230 nm and 228 nm, corresponding energy band gaps of 4.80 eV and 4.90 eV respectively. The above data indicate that Na$_3$Rb$_6$(CO$_3$)$_3$(NO$_3$)$_2$X·6H$_2$O are potentially capable of UV region applications, and may have relatively large laser damage threshold.

Theoretical Calculations. To further understand the relationship between the electronic structure and optical properties of Na$_3$Rb$_6$(CO$_3$)$_3$(NO$_3$)$_2$X·6H$_2$O, theoretical calculation was performed based on DFT. The calculated band structure (Figure S10) shows that Na$_3$Rb$_6$(CO$_3$)$_3$(NO$_3$)$_2$Br·6H$_2$O and Na$_3$Rb$_6$(CO$_3$)$_3$(NO$_3$)$_2$Cl·6H$_2$O are direct band-gap compounds with the valence band maximum (VBM) and the conduction band minimum (CBM) at G point. The GGA-PBE band gaps of Na$_3$Rb$_6$(CO$_3$)$_3$(NO$_3$)$_2$Br·6H$_2$O and Na$_3$Rb$_6$(CO$_3$)$_3$(NO$_3$)$_2$Cl·6H$_2$O are calculated to be 1.77 eV and 1.85 eV, respectively, which is smaller than that of the measured value because of the discontinuity of the exchange-correlation functional.

To understand the composition and origination of the electronic structures, the total density of states (TDOS) and projected density of states (PDOS) are obtained (Figure S10). As shown in Figure S10, for Na$_3$Rb$_6$(CO$_3$)$_3$(NO$_3$)$_2$Br·6H$_2$O, O-2p, C-2p, Rb-4p, Rb-4s and Br-3p states mainly occupy the gap from −6 to −1 eV. The VBM of Na$_3$Rb$_6$(CO$_3$)$_3$(NO$_3$)$_2$Br·6H$_2$O is mainly composed of O-2p, N-2p, Rb-4s, Rb-4p, Na-2p, and a small amount of Br-s orbitals; the CBM of Na$_3$Rb$_6$(CO$_3$)$_3$(NO$_3$)$_2$Br·6H$_2$O is mainly composed of Rb-s as well as Br-s orbitals. For Na$_3$Rb$_6$(CO$_3$)$_3$(NO$_3$)$_2$Cl·6H$_2$O (Figure S10), it is mainly occupied by the O-2p, C-2p, Rb-4p, Rb-4s and Cl-3p states from −6 to −1 eV. The VBM of Na$_3$Rb$_6$(CO$_3$)$_3$(NO$_3$)$_2$Cl·6H$_2$O is dominated by O-2p and H-1s states. The CBM of Na$_3$Rb$_6$(CO$_3$)$_3$(NO$_3$)$_2$Cl·6H$_2$O is mainly dominated by N-2p, O-2p and a little part from Na-2p, Rb-4p, and Rb-4s orbitals. It is well known that, the electronic transition from the VBM to the CBM near the Fermi level determines the optical performance of optical materials. Thus, the linear optical properties of Na$_3$Rb$_6$(CO$_3$)$_3$(NO$_3$)$_2$X·6H$_2$O are mainly determined by the π-conjugated [CO$_3$]$^{2-}$ and [NO$_3$]$^-$ groups.
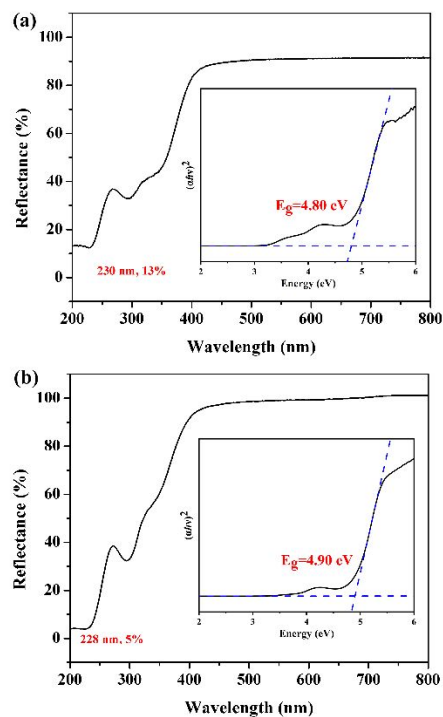
Figure 4 UV-vis diffuse reflectance spectra of (a) Na$_3$Rb$_6$(CO$_3$)$_3$(NO$_3$)$_2$Br·6H$_2$O and (b) Na$_3$Rb$_6$(CO$_3$)$_3$(NO$_3$)$_2$Cl·6H$_2$O.
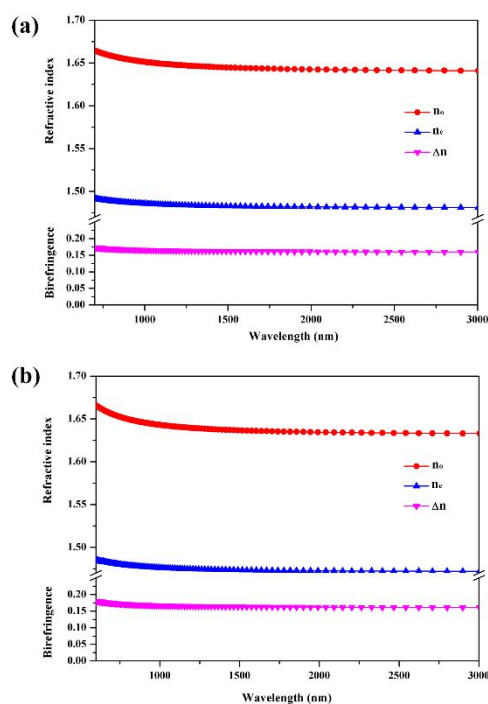
Figure 5 The calculated refractive index and birefringence curves of (a) $Na_3Rb_6(CO_3)_3(NO_3)_2Br·6H_2O$ and (b) $Na_3Rb_6(CO_3)_3(NO_3)_2Cl·6H_2O$.
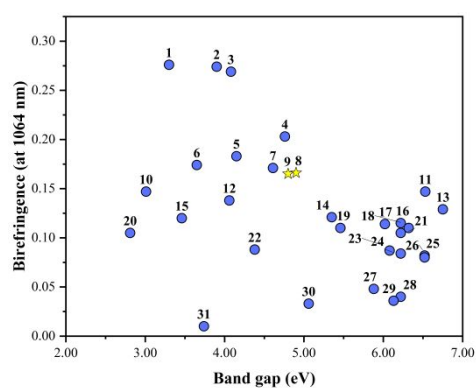
No.	Molecular formula	No.	Molecular formula
1	$Pb_6O_4(BO_3)(NO_3)$	17	$NaZnCO_3(OH)$
2	$KPb_2(CO_3)_2F$	18	$LiKCO_3$
3	$In(IO_3)_2(NO_3)$	19	$KCdCO_3F$
4	$La(OH)_2NO_3$	20	$Cs_3VO(O_2)_2CO_3$
5	$CsPbCO_3F$	21	$KY(CO_3)_2$
6	$Pb_2(BO_3)(NO_3)$	22	$Lu_8O(CO_3)_3(OH)_{15}Br$
7	$NaZnCO_3F$	23	$Zn(NH_3)CO_3$
8	$Na_3Rb_6(CO_3)_3(NO_3)_2Cl·6H_2O$	24	$Na_2Gd(CO_3)F_3$
9	$Na_3Rb_6(CO_3)_3(NO_3)_2Br·6H_2O$	25	$Ca_2Na_3(CO_3)_3F$
10	$Cs_2Pb(NO_3)_2Br_2$	26	$Ba_2NO_3(OH)_3$
11	$LiZn(OH)CO_3$	27	$Ba_3(BO_3)(CO_3)F$
12	$Na_4Zn(CO_3)_3$	28	$(NH_4)_2Ca_2Y_4(CO_3)_9·H_2O$
13	$RbMgCO_3F$	29	$Cs_3B_8O_{13}(NO_3)$
14	$RbCdCO_3F$	30	$Ba_2B_5O_8(OH)_2(NO_3)·3H_2O$
15	$Sr_3[SnOSe_2][CO_3]$	31	$Na_{10}Cd(NO_3)_4(SO_3S)_4$
16	$RbCaCO_3F$		

Figure 6 Birefringences and band gaps statistics of selected carbonates and nitrates.

Linear optical properties. The linear optical properties can be obtained by using the dielectric function, $ε(ω)=ε_1(ω)+iε_2(ω)$. The obtained curve of birefringence versus wavelength is shown in Figure 5. The calculated refractive indices and birefringence curves reveal that $Na_3Rb_6(CO_3)_3(NO_3)_2X·6H_2O$ are negative uniaxial crystals. Their birefrigence value are 0.165 and 0.166 at 1064 nm for $Na_3Rb_6(CO_3)_3(NO_3)_2Br·6H_2O$ and $Na_3Rb_6(CO_3)_3(NO_3)_2Cl·6H_2O$.

A real-space atom-cutting (RSAC) method has been used to intuitively exhibit contribution of $[CO_3]^{2-}$ and $[NO_3]^-$ groups. Following the rule of keeping the cutting spheres in contact and avoiding overlap, the cutting radii are set to be 1.48 Å (Rb), 1.25 Å (Na), 1.60 Å(C), 1.23 Å (N), 0.35 Å (H), 1.10 Å (O), 1.55 Å (Br) and 1.50 Å (Cl). Table S8 shows that the main contribution to the birefringence is derived from $[CO_3]^{2-}$ and $[NO_3]^-$ groups. From the birefringence of the decomposed groups, $[NO_3]^-$ exhibits a birefringence (0.121 at 1064 nm) larger than $[CO_3]^{2-}$ (~0.090 at 1064 nm).

The birefringence of $Na_3Rb_6(CO_3)_3(NO_3)_2Br·6H_2O$ was preliminarily evaluated using the polarized light microscope (Figure S11). The measured direction was chosen randomly and the average thickness of selected crystal is ~7 μm with an optical path difference of 855 nm at 546 nm. So, the corresponding birefringence of $Na_3Rb_6(CO_3)_3(NO_3)_2Br·6H_2O$ along the measured direction is ~0.12, close to the value of $Na_3Rb_6(CO_3)_3(NO_3)_2Cl·6H_2O$ reported in reference 53.

Birefringence and band gap are important criteria for UV birefringent crystals, however, they are essentially opponent. Figure 6 shows the birefringences and band gaps of some carbonates and nitrates (see Table S9 for detailed values), and it can be seen that both properties of $Na_3Rb_6(CO_3)_3(NO_3)_2X·6H_2O$ have relatively well balanced linear optical properties.

Conclusions

In summary, we succeeded in enabling $[CO_3]^{2-}$ and $[NO_3]^-$ groups to co-exist in one structure, and obtained two isostructural compounds $Na_3Rb_6(CO_3)_3(NO_3)_2Br·6H_2O$ and $Na_3Rb_6(CO_3)_3(NO_3)_2Cl·6H_2O$. Although both compounds were characterized in this work, the synthesis and properties of $Na_3Rb_6(CO_3)_3(NO_3)_2Br·6H_2O$ were paid more attention. In the structure of $Na_3Rb_6(CO_3)_3(NO_3)_2Br·6H_2O$, $[NaO_7]^{13-}$ provides five equatorial O atoms, which help $[CO_3]^{2-}$ and $[NO_3]^-$ groups arrange in the coplanar manner, resulting in the most favorable superposition of their anisotropic polarization. Benefiting from the optimized crystal structure, $Na_3Rb_6(CO_3)_3(NO_3)_2Br·6H_2O$ owns a large birefringence of 0.165 at 1064 nm based on theoretical calculations. And the experimental birefringence is about 0.12 at 546 nm. In addition, its UV cut-off edges can reach 230 nm. The desired balance between the birefringence and band gap proves that $Na_3Rb_6(CO_3)_3(NO_3)_2Br·6H_2O$ could be promising UV birefringent crystal. Furthermore, it is noticed that a moderate ionic radius and a suitable radius ratio of cations are essential for the formation of equatorial O atoms, so the selection of an appropriate cation plays a pivotal role in design and synthesis of optical materials based on planar

groups. The successful synthesis of the carbonate nitrate gives more possibilities for exploring new compounds, and we expect that our study on the structure-properties relationship will contribute to the discovery of more novel functional crystal materials.

Conflicts of interest

There are no conflicts to declare.

Acknowledgements

Notes and references

1. C. Lin, A. Zhou, W. Cheng, N. Ye and G. Chai, *J. Phys. Chem. C*, 2019, **123**, 31183-31189.
2. S. Niu, G. Joe, H. Zhao, Y. Zhou, T. Orvis, H. Huyan, J. Salman, K. Mahalingam, B. Urwin, J. Wu, Y. Liu, T. E. Tiwald, S. B. Cronin, B. M. Howe, M. Mecklenburg, R. Haiges, D. J. Singh, H. Wang, M. A. Kats and J. Ravichandran, *Nat. Photon.*, 2018, **12**, 392-396.
3. H. Yang, H. Jussila, A. Autere, H. Komsa, G. Ye, X. Chen, T. Hasan and Z. Sun, *ACS Photonics*, 2017, **4**, 3023-3030.
4. H. Liu, H. Wu, H. Yu, Z. Hu, J. Wang and Y. Wu, *J. Mater. Chem. C*, 2021, **9**, 15321-15328.
5. L. Liu, B. Zhang, P. S. Halasyamani and W. Zhang, *J. Mater. Chem. C*, 2021, **9**, 6491-6497.
6. G. Ghosh, *Opt. Commun.*, 1999, **163**, 95-102.
7. G. Zhou, J. Xu, X. Chen, H. Zhong, S. Wang, K. Xu, P. Deng and F. Gan, *J. Cryst. Growth*, 1998, **191**, 517-519.
8. F. Sedlmeir, R. Zeltner, G. Leuchs and H. G. Schwefel, *Opt. Express*, 2014, **22**, 30934-30942.
9. C. Huang, M. Mutailipu, F. Zhang, K. J. Griffith, C. Hu, Z. Yang, J. M. Griffin, K. R. Poeppelmeier and S. Pan, *Nat. Commun.*, 2021, **12**, 2597.
10. X. Li and G. Yang, *Inorg. Chem.*, 2022, **61**, 10205-10210.
11. S. Han, Y. Wang, B. Zhang, Z. Yang and S. Pan, *Inorg. Chem.*, 2018, **57**, 873-878.
12. C. Huang, G. Han, H. Li, F. Zhang, Z. Yang and S. Pan, *Dalton Trans.*, 2019, **48**, 6714-6717.
13. S. Bai, X. Zhang, B. Zhang, L. Li and Y. Wang, *Inorg. Chem.*, 2021, **60**, 10006-10011.
14. X. Shi, W. Zhang, W. Cai, S. Han, Z. Yang and S. Pan, *Inorg. Chem.*, 2021, **60**, 12565-12572.
15. X. Chen, B. Zhang, F. Zhang, Y. Wang, M. Zhang, Z. Yang, K. R. Poeppelmeier and S. Pan, *J. Am. Chem. Soc.*, 2018, **140**, 16311-16319.
16. R. Zhang, X. Su, J. Zhang, D. Wen and Y. Huang, *Chem. Commun.*, 2022, **58**, 10182-10185.
17. R. Guo, X. Jiang, S. Guo, M. Xia, L. Liu, Z. Lin and X. Wang, *Inorg. Chem.*, 2022, **61**, 7624-7630.
18. C. Jin, F. Li, B. Cheng, H. Qiu, Z. Yang, S. Pan and M. Mutailipu, *Angew. Chem. Int. Ed.*, 2022, **61**, e202203984.
19. Y. Li, X. Chen and K. M. Ok, *Chem. Commun.*, 2022, **58**, 8770-8773.
20. S. Li, X. Liu, H. Wu, Z. Song, H. Yu, Z. Lin, Z. Hu, J. Wang and Y. Wu, *Chem. Sci.*, 2021, **12**, 13897-13901.
21. W. Zhang, J. Huang, S. Han, Z. Yang and S. Pan, *J. Am. Chem. Soc.*, 2022, **144**, 9083-9090.
22. L. Cao, Y. Song, G. Peng, M. Luo, Y. Yang, C. Lin, D. Zhao, F. Xu, Z. Lin and N. Ye, *Chem. Mater.*, 2019, **31**, 2130-2137.
23. Y. Long, X. Dong, H. Zeng, Z. Lin and G. Zou, *Inorg. Chem.*, 2022, **61**, 4184-4192.
24. R. Li, *Z. Kristallogr.*, 2013, **228**, 526-531.
25. X. Dong, L. Huang, Q. Liu, H. Zeng, Z. Lin, D. Xu and G. Zou, *Chem. Commun.*, 2018, **54**, 5792-5795.
26. Y. Song, M. Luo, C. Lin and N. Ye, *Chem. Mater.*, 2017, **29**, 896-903.
27. G. Wang, M. Luo, N. Ye, C. Lin and W. Cheng, *Inorg. Chem.*, 2014, **53**, 5222-5228.
28. K. Kobayashi, T. Ikeda, N. Hiyoshi and Y. Sakka, *CrystEngComm*, 2014, **16**, 10080-10088.
29. M. Abudoureheman, L. Wang, X. Zhang, H. Yu, Z. Yang, C. Lei, J. Han and S. Pan, *Inorg. Chem.*, 2015, **54**, 4138-4142.
30. L. Liu, Y. Yang, J. Huang, X. Dong, Z. Yang and S. Pan, *Chem. Eur. J.*, 2017, **23**, 10451-10459.
31. C. Huang, F. Zhang, S. Cheng, Z. Yang, H. Li and S. Pan, *Chem. Eur. J.*, 2020, **26**, 16628-16632.
32. Q. Zhang, F. Zhang, F. Li, S. Han, Z. Yang and S. Pan, *Eur. J. Inorg. Chem.*, 2021, **2021**, 1297-1304.
33. S. Bai, D. Yang, B. Zhang, L. Li and Y. Wang, *Dalton Trans.*, 2022, **51**, 3421-3425.
34. J. Song, C. Hu, X. Xu, F. Kong and J. Mao, *Angew. Chem. Int. Ed.*, 2015, **127**, 3750-3753.
35. I. Bernal and J. Cetrullo, *Struct. Chem.*, 1990, **1**, 227-234.
36. H. K. Mahtani, S. Chang, J. R. Ruble, I. N. L. Black and P. B. Stein, *Inorg. Chem.*, 1993, **32**, 4976-4978.
37. A. Barnabe´, F. Letouze´, D. Pelloquin, A. Maignan, M. Hervieu and B. Raveau, *Chem. Mater.*, 1997, **9**, 2205-2211.
38. A. Norlund Christencen and R. G. Hazell, *Acta Chem. Scand.*, 1999, **53**, 399-402.
39. J. Zhu, H. Wu and A. Le Bail, *Solid State Sci.*, 1999, **1**, 55-62.
40. Y. Li, S. V. Krivovichev and P. C. Burns, *J. Solid State Chem.*, 2000, **153**, 365-370.
41. G. R. Blake, A. R. Armstrong, E. Sastre, W. Zhoua and P. A. Wright, *Mate. Res. Bull.*, 2001, **36**, 1837-1845.
42. Y. Li and P. C. Burns, *J. Solid State Chem.*, 2002, **166**, 219-228.
43. A. Le Bail, *Acta Cryst.*, 2013, **E69**, i42-i43.
44. S. N. Vorob'eva, I. A. Baidina and I. V. Korol'kov, *J. Struct. Chem.*, 2016, **57**, 1588-1592.
45. J. Jiao, F. Liang, C. Li, T. Han, W. Zhao, Y. She, N. Ye, Z. Hu and Y. Wu, *Inorg. Chem.*, 2022, **61**, 11471-11477.
46. Y. Deng, L. Huang, X. Dong, L. Wang, K. M. Ok, H. Zeng, Z. Lin and G. Zou, *Angew. Chem. Int. Ed.*, 2020, **59**, 21151-21156.
47. J. Guo, A. Tudi, S. Han, Z. Yang and S. Pan, *Angew. Chem. Int. Ed.*, 2021, **60**, 24901-24904.
48. H. Tang, R. Fu, Z. Ma and X. Wu, *Inorg. Chem.*, 2021, **60**, 17364-17370.
49. H. Yu, W. Zhang, J. Young, J. M. Rondinelli and P. S. Halasyamani, *J. Am. Chem. Soc.*, 2016, **138**, 88-91.
50. J. Jiao, M. Cheng, R. Yang, Y. Yan, M. Zhang, F. Zhang, Z. Yang and S. Pan, *Angew. Chem. Int. Ed.*, 2022, **61**, e202205060.
51. G. Shi, F. Zhang, B. Zhang, D. Hou, X. Chen, Z. Yang and S. Pan, *Inorg. Chem.*, 2017, **56**, 344-350.

52. Y. Jia, X. Zhang, Y. Chen, X. Jiang, J. Song, Z. Lin and X. Zhang, *Inorg. Chem.*, 2022, **61**, 15368-15376.
53. M. Cheng, W. Jin, Z. Yang and S. Pan, *Chem. Sci.*, 2022, **13**, 13482-13488.
54. SAINT, version 7.60A Bruker Analytical X-ray Instruments, Inc.: Madison, WI, 2008.
55. G. M. Sheldrick, *Acta Cryst.*, 2015, **71**, 3-8.
56. A. L. Spek, *J. Appl. Cryst.*, 2003, **36**, 7-13.
57. S. J. Clark, M. D. Segall, C. J. Pickard, P. J. Hasnip, M. I. J. Probert, K. Refson and M. C. Payne, *Z. Kristallogr.*, 2005, **220**, 567-570.
58. J. S. Lin, A. Qteish, M. C. Payne and V. Heine, *Phys. Rev. B: Condens. Matter Mater. Phys.*, 1993, **47**, 4174-4180.
59. A. M. Rappe, K. M. Rabe, E. Kaxiras and J. D. Joannopoulos, *Phys. Rev. B: Condens. Matter Mater. Phys.*, 1990, **41**, 1227-1230.
60. J. P. Perdew, K. Burke and M. Ernzerhof, *Phys. Rev. Lett.*, 1996, **77**, 3865-3868.
61. I. D. Brown and D. Altermatt, *Acta Cryst.*, 1985, **41**, 244-247.
62. N. E. Brese and M. O'Keeffe, *Acta Cryst.*, 1991, **47**, 192-197.
63. G. Peng, Y. Tang, C. Lin, D. Zhao, M. Luo, T. Yan, Y. Chen and N. Ye, *J. Mater. Chem. C*, 2018, **6**, 6526-6533.
64. G. Zou, N. Ye, L. Huang and X. Lin, *J. Am. Chem. Soc.*, 2011, **133**, 20001-20007.
65. L. Huang, G. Zou, H. Cai, S. Wang, C. Lin and N. Ye, *J. Mater. Chem. C*, 2015, **3**, 5268-5274.
66. T. T. Tran, J. He, J. M. Rondinelli and P. S. Halasyamani, *J. Am. Chem. Soc.*, 2015, **137**, 10504-10507.
67. G. Zou, G. Nam, H. G. Kim, H. Jo, T. S. You and K. M. Ok, *RSC Adv.*, 2015, **5**, 84754-84761.
68. T. T. Tran, P. S. Halasyamani and J. M. Rondinelli, *Inorg. Chem.*, 2014, **53**, 6241-6251.
69. G. Zou, C. Lin, H. G. Kim, H. Jo and K. M. Ok, *Crystals*, 2016, **6**, 42.
70. A. Adam and V. Cirpus, *Z. Anorg. Allg. Chem.*, 1996, **622** 2023-2030.
71. B. Albert, J. Arlt and M. Jansen, *Z. Anorg. Allg. Chem.*, 1992, **607**, 13-18.
72. A. V. Yatsenko, S. G. Zhukov, V. A. Dyakov and H. Schenk, *Acta Cryst.*, 1996, **C52**, 1-3.
73. Q. Liu, Z. Li, Y. Wang, X. Su, Z. Yang and S. Pan, *Dalton Trans.*, 2017, **46**, 6894-6899.
74. C. Bois, G. Papin and M. Philoche-Levisalles, *Revue de Chimie Minérale*, 1984, **21**, 152-158.